Features of criticality are asymmetric in the zebrafish habenula

Suryadi[1,2,3], Mahathi Ramaswamy[3], Suresh Jesuthasan[3,4] & Lock Yue Chew[1,2]
1: School of Physical & Mathematical Sciences, Nanyang Technological University Singapore.
2: Complexity Institute, Nanyang Technological University Singapore.
3: Lee Kong Chian School of Medicine, Nanyang Technological University Singapore.
4: Institute of Molecular and Cell Biology, Singapore.
Correspondence and requests for materials should be addressed to
L.Y.C. (email: lockyue@ntu.edu.sg) and S.J. (email: sureshj@ntu.edu.sg)

The habenula is an evolutionarily conserved structure of the vertebrate brain essential for behavioural flexibility and mood control. It is spontaneously active and is able to access diverse states upon exposure to stimulation. Information processing in the habenula can potentially be understood through criticality, which describes a system at the boundary between different dynamical states. Here we analyze two-photon calcium imaging time-series of a single plane of the dorsal habenula of larval zebrafish for statistical features of criticality, namely avalanche distributions and shape collapse. We find that the dorsal habenula, which has left-right asymmetry in connectivity and function, displays asymmetric features of criticality, with the left dorsal habenula being at or near a critical state, while the right side is not. Deviations from theoretical predictions were understood through a branching model to result from subsampling. These observations provide evidence that a sub-cortical region of the vertebrate brain operates at a critical state in the intact animal.

Introduction

A defining feature of neural circuits is their flexibility. Although anatomical connectivity does not change rapidly in a mature animal, functional connectivity can change within seconds, enabling animals to quickly alter their behavior to deal with changing circumstances and to learn. The flexibility of neural circuits is made possible in part by the action of neuromodulators.[1–3] To ensure that functional connectivity is appropriate for a given condition, the release of neuromodulators is normally tied to a variety of factors, such as internal state of the animal, external cues and perceived reward.

The habenula is an epithalamic structure that receives indirect input from several sensory systems,[4–6] is stimulated by punishment or absence of an expected reward,[7–9] and has activity that is dependent on the circadian clock[10] and stress levels.[11] It sends output to a number of structures, including the raphe[12] and the rostro-medial tegmental nucleus,[13] which regulate the release of serotonin and dopamine respectively. Thus, the habenula is well positioned to coordinate release of broadly acting neuromodulators based on a variety of factors. The importance of the habenula is illustrated by a large range of defect seen in animals with a lesioned habenula, including an inability to cope with changing circumstances[14] or learn effectively.[15,16]

How does the habenula process information to efficiently influence behaviour? Calcium imaging in zebrafish indicates that neural activity in the habenula is sensitive to various features of sensory input. Different concentrations of odours,[17] as well as wavelengths[18] or levels of ambient illumination[5] trigger different patterns of activity. This can be represented as trajectories in state space, with reproducible trajectories for each stimulus, indicating that sensory stimuli is represented by population activity. Additionally, habenula neurons constantly fire action potentials, even in the absence of sensory stimulation. This was demonstrated in rats, using electrical recordings of brain slices, and has also been found to be the case in the zebrafish, using two-photon calcium imaging of tethered animals,[19,20] or CaMPARI-based labelling of freely swimming fish.[21] These features – constant activity and the ability to occupy multiple different states - raise the possibility that the habenula may be operating at criticality.

Criticality optimizes information processing by maximizing information transmission,[22] sensitivity to input,[23,24] information capacity,[25] the dynamic range of the network,[23–26] as well as the fidelity and variability of the information transmitted.[25] These benefits were not only demonstrated in computational models; but have also been ob-

served in both in vitro and in vivo experiments involving cortical neurons.[24–26] Criticality also provides another context for the seemingly incessant activity that runs in the habenula, as instead of being a background chatter of the network, it serves a definite purpose of poising the system into a critical state. Here, using the zebrafish, which has an easily accessible epithalamus, we ask whether the habenula could be at a critical state in vivo. To evaluate this, we investigate the statistical physics of neuronal avalanches. In particular, we examine the form of the probability distribution of the size and duration of the avalanches. If the habenula is at a critical state, these distributions should have the form of a power law.[22,27–29] In addition, we also examine the scaling laws and universal function, which are more rigorous hallmarks of criticality.[27–29] We focus here on the dorsal habenula, which is asymmetric in terms of input neurons as well as channels and receptors. Given that this will affect neural dynamics, we performed analysis on the left and right habenula separately. Our analysis indicates that the dorsal left habenula operates at criticality.

Results

Avalanche Distributions.

We recorded neural activity using two-photon calcium imaging of the dorsal habenula of the larval zebrafish in the absence of sensory stimuli (i.e. in darkness). Any neural activity in these conditions was assumed to be spontaneous. From each recording we then identified the neurons and inferred the corresponding neural spikes (see Methods), which allowed us to study the population behavior of the habenula through neuronal spike avalanches. For a critical system, avalanches of size S and duration T are known to form power law distributions:[28]

$$P(S) \sim S^{-\tau} \tag{1}$$

$$P(T) \sim T^{-\alpha}, \tag{2}$$

where mean field results yielded τ and α valued at -1.5 and -2 respectively.[30]

The nature of the experimental setup was such that each recording was limited both spatially (i.e. a single plane of neurons, as more planes would reduce the quality of the recording) and temporally (up to 15 minutes per recording, due to drift). These factors led to a relatively small sample size of avalanches per recording. To circumvent this problem, we combined the histograms obtained from several recordings at identical sampling rates, by summing the histogram counts for each observation. The noisy nature of the data necessitated the binning of data, after which a power law behavior became apparent (see Figure 1).

Table 1 shows the power law exponents (τ for avalanche size and α for avalanche duration) obtained for the left dorsal habenula (LdHb) and right dorsal habenula (RdHb) for different sampling rates along with their associated KS statistics (see Methods). For the 7.0 Hz RdHb recording, α (and therefore the subsequent goodness of fit and likelihood ratio tests) could not be determined as the distribution does not display any power law-like regime. All distributions for LdHb except the 7.0 Hz avalanche size distribution passed the power law goodness of fit test,[31] while only half the distributions (4 out of 8) for RdHb passed the test. Likelihood ratio test favors exponential distribution for both LdHb and RdHb 7.0 Hz size distributions, as well as the 2.0 Hz RdHb duration distribution ($p < 0.10$). For the remaining distributions, the likelihood ratio test either favors power law ($p < 0.10$) or or is unable to determine due to high p-value.[31] The total number of avalanches observed for each dataset as well as the exact p-values obtained for both goodness of fit and likelihood ratio tests can be found in Supplementary Table S1.

We see that the exponents obtained are not close to the predicted mean field values. However, as the power law behavior disappears upon temporally shuffling the neural spike data (see Supplementary Figure S1; likelihood ratio test favors exponential distribution with $p < 0.10$ for all distributions with shuffled data), it is likely that the spatiotemporal correlations suggested by the power law distributions are not due to chance.

Mean Avalanche Size as a Function of Duration.

It is well known that the existence of a power law distribution alone does not necessarily point towards a critical system.[32,33] However, its presence nevertheless provides support to the criticality hypothesis when presented together with other known traits of criticality. One such trait is obtained by collecting avalanches of the same duration and thereby computing the mean avalanche size as a function of duration. This function follows a well-defined form,[27,28] as described by the following expression:

$$\langle S \rangle (T) \sim T^{\beta}, \tag{3}$$

where β is related to both the avalanche distribution exponents τ and α seen in equations (1) and (2) as such:[28]

$$\frac{\alpha - 1}{\tau - 1} = \beta\,. \tag{4}$$

In general, our results trace the shape of a power law function with slightly varying exponents (Figure 2). The exponent β from these plots were computed via a robust linear regression measure known as the Theil-Sen estimator, and

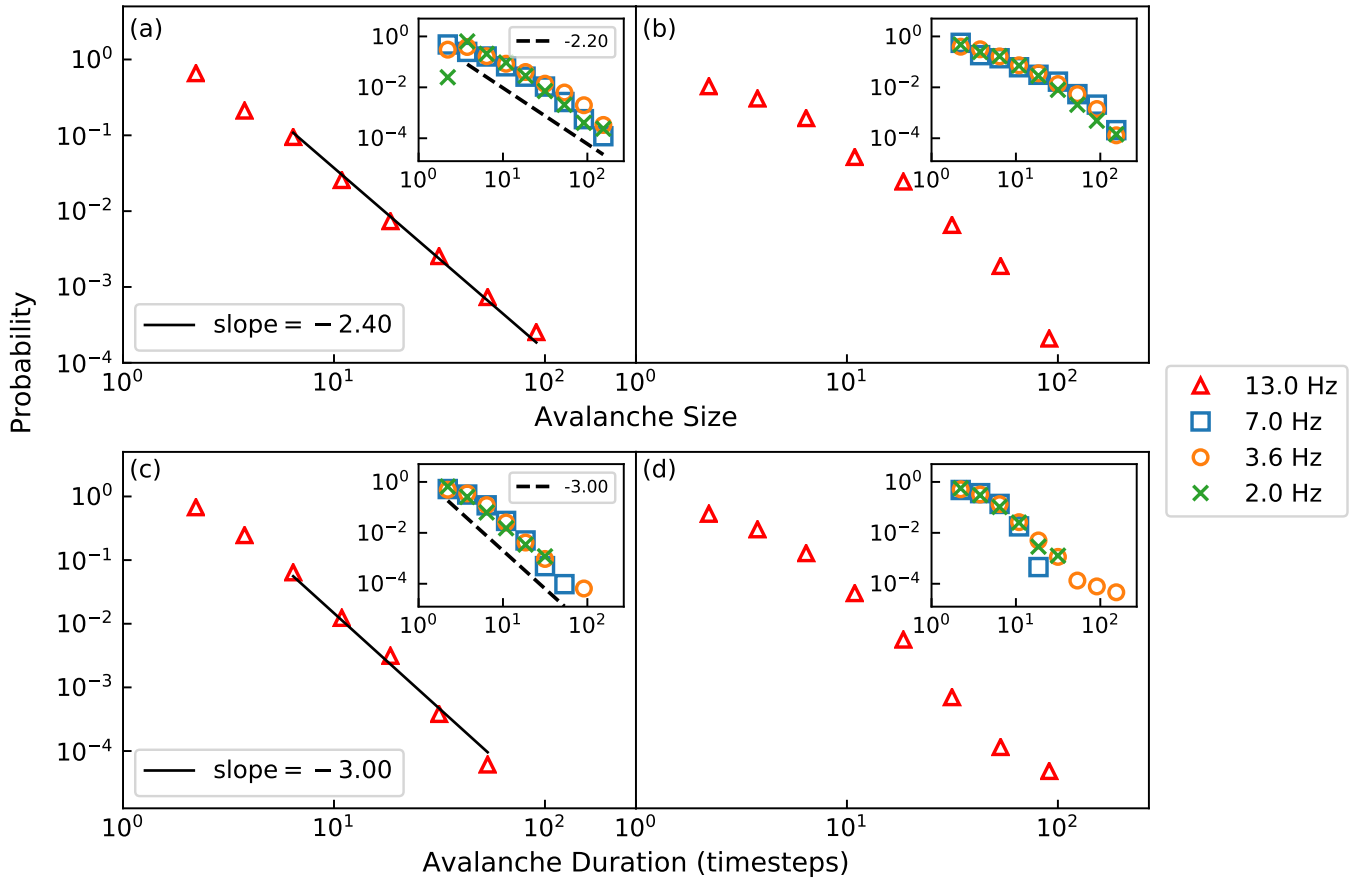

Figure 1: Logarithmically-binned avalanche size and duration distributions for data obtained at the sampling rate of 13.0 Hz. Top: avalanche size distributions for left (a) and right (b) dorsal habenula respectively; bottom: avalanche duration distributions for left (c) and right (d) dorsal habenula respectively. In all plots the inset shows distributions for data obtained at other sampling rates. In general we see that LdHb displays power law regimes in its distributions, while RdHb distributions tend to instead show an exponential-like decay. Table 1 shows the power law statistics obtained from maximum likelihood methods.[31] For all these distributions, time-shuffling the data leads to the abolishment of power law to form exponential distribution (see Supplementary Figure S1).

Sampling Rate (Hz)	LdHb				RdHb			
	Size		Duration		Size		Duration	
	τ	KS	α	KS	τ	KS	α	KS
2.0	2.40 ± 0.17	0.009	2.65 ± 0.26	0.001	2.45 ± 0.23	0.004	2.40 ± 0.16	0.026
3.6	1.50 ± 0.03	0.008	3.05 ± 0.47	0.004	1.60 ± 0.04	0.015	3.00 ± 0.81	0.007
7.0	1.95 ± 0.07	0.021	3.55 ± 0.75	0.009	1.50 ± 0.02	0.017	–	–
13.0	2.35 ± 0.07	0.009	3.05 ± 0.28	0.006	2.05 ± 0.04	0.018	3.30 ± 0.35	0.006

Table 1: Avalanche statistics for binned data categorized by sampling rate for data taken from left dorsal habenula (LdHb) and right dorsal habenula (RdHb). τ and α are the power law exponents of the avalanche size and duration distributions respectively, shown alongside their corresponding KS statistics which measures the distance between the experimental data and power law fit. α for RdHb at 7.0 Hz cannot be determined as the distribution does not have any power law-like regime.

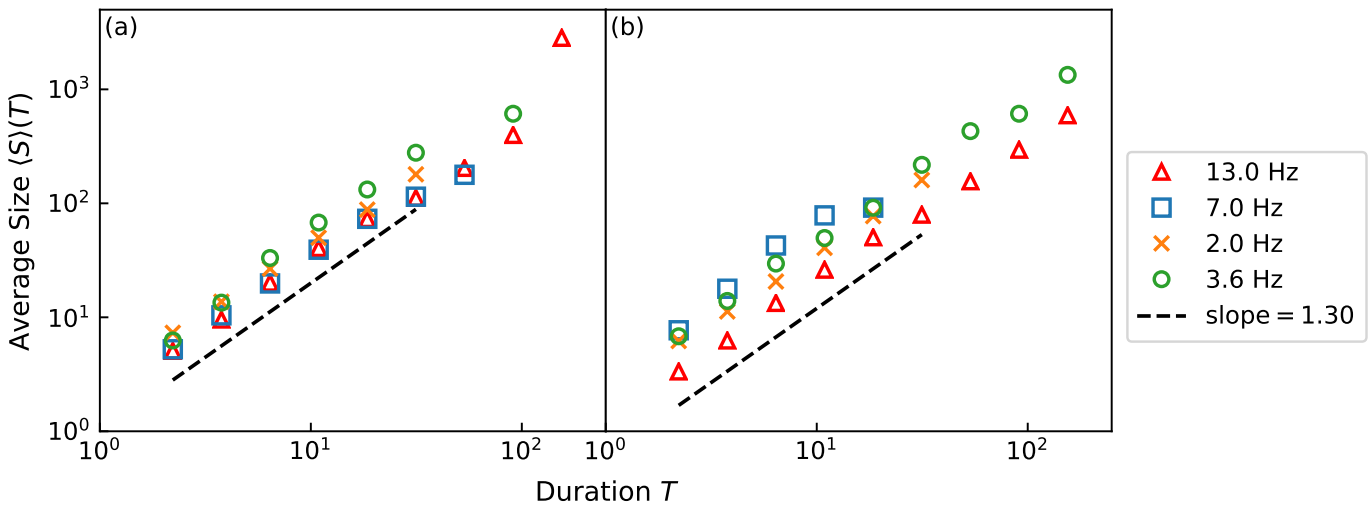

Figure 2: Average avalanche size given duration for avalanche data from the left (a) and right (b) dorsal habenula, both of which largely correspond to a power function with an exponent around 1.3. Time-shuffled data largely retains a power law function, albeit with a different slope (see Supplementary Figure S1).

are shown in Table 2 in the $\beta_{\langle S\rangle(T)}$ column. Here we see that most of the datasets fail to satisfy relation (4). The reason for this will be elucidated later in the section on Simple Branching Model.

Shape Collapse.

One of the more stringent hallmarks of criticality is shape collapse.[28,29] A critical system is scale-invariant, i.e. has no preferred scale, hence avalanches of different scales — from small to large — develop and propagate in a way such that the average size appears more or less the same once the scale is normalized.[27] In neural avalanches, this shape is observed to be approximately parabolic,[28] although its shape need not be perfectly symmetric.[34]

Formally, the average number of spikes $s(t,T)$ for an avalanche of duration T at time t satisfies the following relation:[28,29]

$$s(t,T) \propto T^{\gamma} F(t/T), \tag{5}$$

where $F(t/T)$ is a universal scaling function that describes the temporal profile of the avalanche. To test for the shape collapse, we simply need to plot $s(t,T)T^{-\gamma}$ for all T in normalized time t/T, hence each curve describes the average profile of avalanches of a particular duration T. The exponent γ here is related to the exponent β seen in (3) as follows:[29]

$$\gamma = \beta - 1. \tag{6}$$

Aside from the scale-invariant collapse of the temporal avalanche profile into a parabolic shape, the scaling relation above provides another means of testing for criticality. The shape collapse plots in Figure 3 are obtained by optimizing the value of γ to minimize the variance between the curves in the plots.[29] For convenience, we express γ in terms of β using (6), hence the scaling relation is satisfied when $\beta_{Collapse}$ obtained from scaling collapse agrees with those obtained via the mean avalanche size given duration plots.

Significant statistical fluctuations can enter the analysis in two ways: short avalanches and curves that average over few avalanches. For the former, short avalanches have too few points to accurately trace the actual mean avalanche profile, while for the latter, the computed mean values may not be representative of the actual population mean due to the small sample of avalanches present. We therefore minimize such effects by constraining our analysis to avalanches lasting at least 5 time steps, as well as to durations T that have at least 25 observed avalanches.

In Figure 3, the shape collapse plots for the sampling rate of 2 Hz were not shown as the curves for LdHb did not satisfy our constraints, hence shape collapse analysis could not be performed. The corresponding shape collapse plot at 2 Hz for RdHb can be found in Supplementary Figure S3. For the datasets in Figure 3, we observe results consistent with what would be expected from an avalanching critical system, with the mean avalanche profiles collapsing into a parabolic shape. Such parabolic profiles were lost upon temporally shuffling the data, indicating that the collapse of parabolic avalanche profiles is not due to chance (see Supplementary Figure S2). Interestingly, the results for RdHb turned out to be quite different from LdHb. Firstly only two datasets produce a parabolic shape (3.6 Hz and 7 Hz data); in fact the 3.6 Hz dataset does not collapse well either, which may be due to the small number of curves present, or simply reflecting the fact that the system is not critical.

From Table 2 we see that scaling relation (6) is satisfied for all LdHb datasets where shape collapse analysis is possible, which, along with the successful shape collapse with a parabolic average profile, suggests that LdHb functions at or close to a critical state. On the other hand, the relation is only satisfied for 2 out of the 4 RdHb datasets, which coincidentally are also the datasets that failed to collapse into a parabolic profile, suggesting that in contrast to LdHb, the RdHb does not exist at or close to a critical state.

Simple Branching Model.

So far we have seen that while the shape collapse and the relation between γ and β are in agreement with the criticality hypothesis (at least for the LdHb), the power law distributions yield exponents that are far from mean field predictions, which also fail to satisfy the known scaling relation with respect to β, i.e. equation (4). Noting that our empirical data were obtained by spatially subsampling the system, we construct here a simple branching model to investigate how subsampling affects the analysis.

We base our model on a 3-dimensional square lattice, constructed by stacking 3 planes of 2-dimensional square lattices in the vertical direction, with periodic boundary conditions in all 3 dimensions. Each node in the model represents a neuron, and the dynamics is such that a neural spike has some probability of causing a connected neuron to spike in the next time step. In branching process terminology, the initial neural spike is termed the *ancestor*, while the neural spike induced by the ancestor is called the *descendant*. We impose a critical branching process onto the system in probabilistic terms:[35,36] the average number of descendants generated by one ancestor (also known as the *branching parameter*) is set to be 1. Since each neuron in this 3D square lattice is connected to 6 other neurons, we find that each neural spikes should have a probability p_{spike} of causing each neighbor to spike equal to $1/6$. In practice, however, we find that we need a slightly larger p_{spike} to obtain a branching parameter close to 1 (see Supplementary Figure S4).

The dynamics in the model is such that when the network is quiescent, a random neuron is brought to spike. If any neuron spikes in the current time step, the model is left to evolve as it is without interference. The resulting data would then be analyzed in two ways. Firstly, we fully sample the model and through the time series of the total number of spikes at each time step, analyze the time series so as to obtain avalanche size and duration statistics. This step is to verify that the model does indeed, by the criteria employed in this paper, exist in a critical state. Next, we subsample the model in a way similar to the experimental setup. In particular, we measure only from a single plane, and from there, observe only a subset of neurons present in that plane. We then repeat the same analysis on the time series as in the fully sampled case, and hence we would be in a good position to compare them and observe the effect of subsampling.

Figure 4 shows the results from a simulation where each plane of the lattice was set to be of dimensions 30×30, simulated for $100,000$ timesteps. We take $p_{spike} = 0.1716$, which yielded a branching parameter of 1.001. Identical to our data, we bin the plots logarithmically with base 1.7. Figure 4 shows that the fully sampled case yielded exponents $\tau = 1.50,\ \alpha = 1.80,\ \beta \approx 1.60$. Although the avalanche duration distribution yielded an exponent different from the mean field value of 2, the exponents nevertheless satisfy relation (4). Moreover, the shape collapse resulted in a good parabolic shape, with $\beta = 1.63$, which closely corresponds to the value obtained through the average size given duration plot (therefore satisfying relation (6)). All these factors put together indicate that the system is indeed in a critical state.

We then subsampled 50, 100, and 200 neurons respectively out of the entire network, and we see that the results are similar to our experimental data. In particular, upon subsampling the exponents are increased to around $\tau \approx 2.10,\ \alpha \approx 2.65,\ \beta \approx 1.39$ depending on the extent

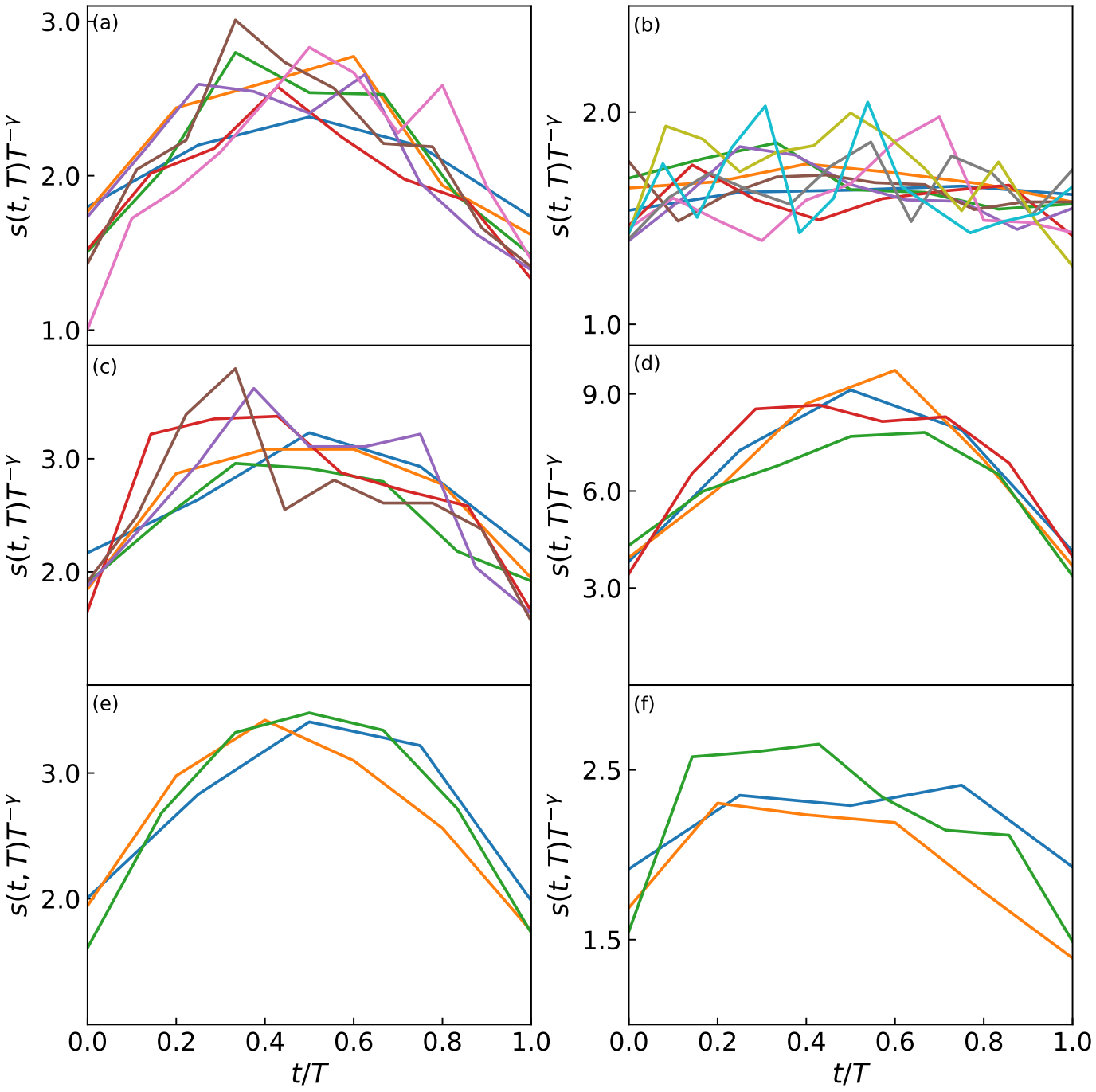

Figure 3: Shape collapse for data of sampling rates 13 Hz (a-b), 7 Hz (c,d), and 3.6 Hz (e,f): left — LdHb, right — RdHb. Here we see that LdHb data collapse into a parabolic shape for all 3 datasets, while RdHb shows one dataset (b) which fails to do so. In all cases, time-shuffled data leads to the abolishment of shape collapse, indicating that the results obtained here are not statistical artifacts (see Supplementary Figure S2).

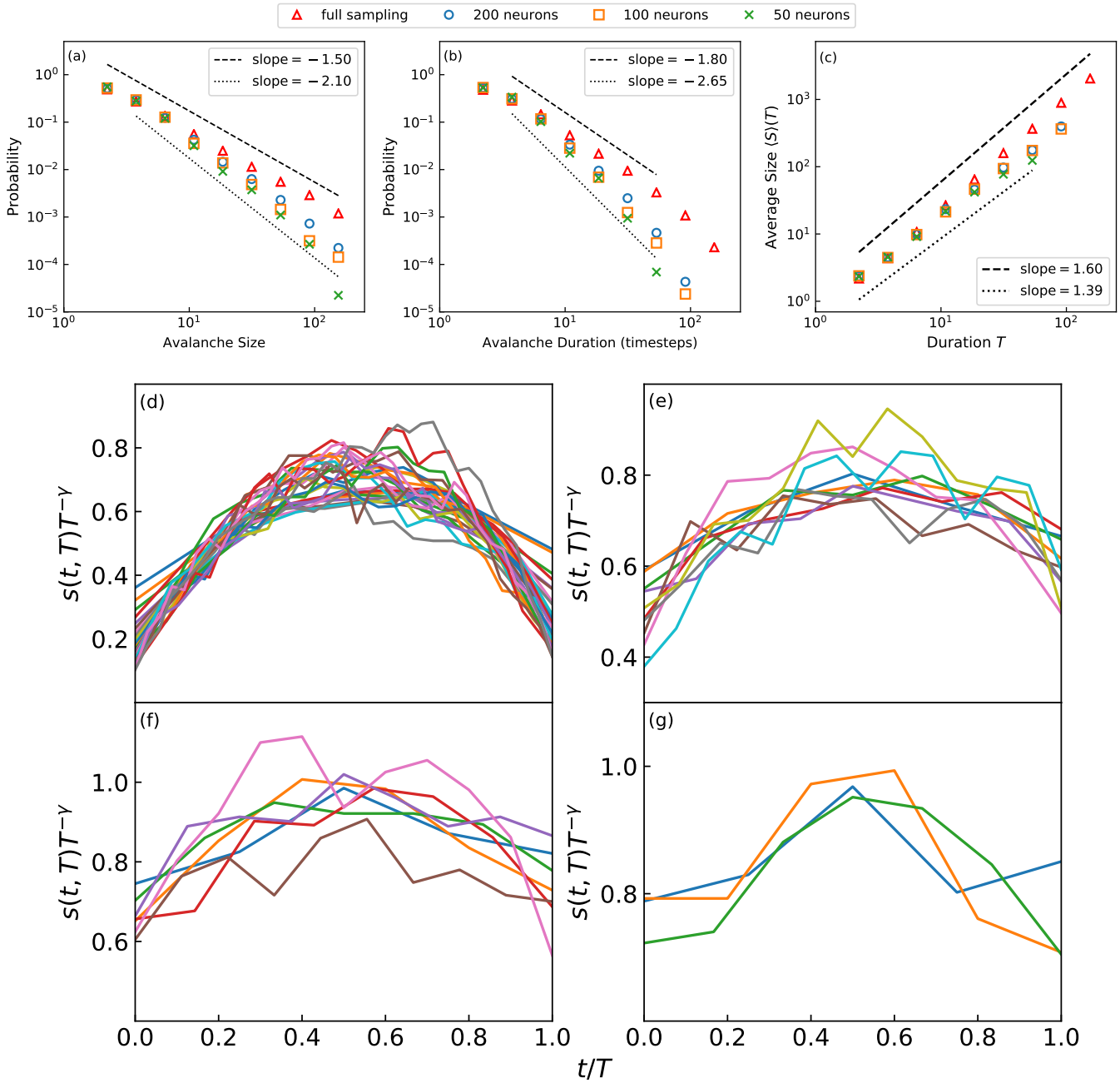

Figure 4: Simulation results with the simple branching model. Top: avalanche size (a), duration (b), and mean size given duration (c) plots with full sampling as well as subsampling. Bottom: shape collapse with full sampling (d) and subsampling [(e): 200 neurons, (f): 100 neurons, (g): 50 neurons].

Sampling Rate (Hz)	LdHb			RdHb		
	$\frac{\alpha-1}{\tau-1}$	$\beta_{\langle S\rangle(T)}$	$\beta_{Collapse}$	$\frac{\alpha-1}{\tau-1}$	$\beta_{\langle S\rangle(T)}$	$\beta_{Collapse}$
2.0	1.18 ± 0.37	1.207 ± 0.083	–	0.97 ± 0.30	1.211 ± 0.079	1.137
3.6	4.10 ± 1.21	1.348 ± 0.249	1.391	3.33 ± 1.70	1.243 ± 0.062	1.438
7.0	2.68 ± 1.06	1.162 ± 0.211	1.140	–	1.520 ± 0.373	1.052
13.0	1.52 ± 0.30	1.193 ± 0.212	1.262	2.19 ± 0.44	1.209 ± 0.057	1.162

Table 2: Table containing the β exponents obtained from relation (4), the mean size given duration plot, as well as shape collapse. $\beta_{Collapse}$ for 2.0 Hz LdHb data is absent as shape collapse could not be performed for that dataset, while $\frac{\alpha-1}{\tau-1}$ could not be computed for the 7.0 Hz RdHb dataset as α could not be determined (see Table 1). We see that β obtained from $\langle S\rangle(T)$ and shape collapse agree for LdHb. On the other hand, this same is true only for the 2 and 13.0 Hz dataset for RdHb, for which the shape collapse failed (see Supplementary Figure S3 and Figure 3). Most of the $\frac{\alpha-1}{\tau-1}$ values, on the other hand, do not agree with the β values, hence relation (4) is not satisfied in general for both LdHb and RdHb.

#Neurons	τ	α	$\frac{\alpha-1}{\tau-1}$	$\beta_{\langle S\rangle(T)}$	$\beta_{Collapse}$
All	1.50 ± 0.01	1.80 ± 0.02	1.60 ± 0.07	1.649 ± 0.037	1.633
50	2.35 ± 0.16	2.80 ± 0.31	1.33 ± 0.44	1.378 ± 0.261	1.345
100	2.15 ± 0.09	2.75 ± 0.20	1.52 ± 0.32	1.419 ± 0.093	1.351
200	1.80 ± 0.03	2.40 ± 0.11	1.75 ± 0.21	1.389 ± 0.062	1.461

Table 3: Critical exponents obtained from the simple branching model. While the fully sampled model displays agreement between the β values in the last three columns, we see that subsampling may cause this agreement to be abolished.

of subsampling, and we see that relation (4) is no longer always satisfied. Naturally, the exact values of the exponents, and therefore their agreement with relation (4), is subject to random fluctuations due to the indeterministic nature of the subsampling process. Moreover, likelihood ratio test on these subsampled datasets may also fail to conclude on whether power law or exponential distribution provides a better fit (or in some cases, actually favoring exponential distribution), which also corresponds to what we have observed. Interestingly, β exponents obtained from shape collapse are still within the tolerance of those obtained from the average size given duration plots, which implies that relation (6) is satisfied, which again presents the same situation as our experimental data. We note here however that this needs not necessarily always be the case; subsampling may lead to cases where relation (6) is not satisfied, even if the underlying network is critical. Despite so, our simulations have shown that the shape collapse plots nevertheless produce a good parabolic shape even in cases where the relation is not satisfied (plots not shown, but are similar to what we see in Figure 4). This characteristic, therefore, remains as a viable necessary criterion to infer criticality in the system. Our LdHb data, which both produce the parabolic shape and satisfy the associated scaling relation, therefore, satisfy this criterion. More importantly, these results show that the significantly larger exponents of the power law distributions can be explained by subsampling.

Discussion

To investigate the possibility of criticality in the zebrafish dorsal habenula, we inspected avalanche size and duration distributions and found exponents that deviate from mean field results. We then looked at the mean avalanche size as a function of duration, and found that the scaling relation (4) is not satisfied. Upon further investigation using a simple branching model, we found that this may result from subsampling, i.e. a critical system can display these seemingly non-critical behavior simply because it is subsampled. Nevertheless, a subsampled critical system still displays a parabolic shape collapse, such that the relation (6) is often, though not always satisfied. The shape collapse observed in the LdHb display a good agreement with these findings, suggesting that this region of the habenula functions at or close to a critical state. If true, this work would present the first observation of criticality in the vertebrate brain outside the cortex.

The anatomical and functional asymmetry of the LdHb and RdHb of zebrafish is well established.[37–39] Our results suggest an additional facet of asymmetry: the left and right dHb exist in different dynamical states, with the left being at or near a critical state, while the right is in a non-critical state, at least in the present experimental conditions. If this is indeed the case, then both sides of the dHb may operate as distinct, independent subunits. While information may be

shared between the two sides across the habenula commissure, the actual computation and processing may be done independently of each other. A question that may arise is why one side of the habenula may seem to be critical, while the other side is not, despite the many benefits being ascribed to a critical state. Interestingly, this asymmetry could also prove beneficial; it has been shown that the presence of both critical and non-critical (specifically, subcritical) components maximizes both the sensitivity as well as specificity of the network.[40] The subcritical component is required for the latter owing to the fact that while criticality maximizes the sensitivity of the network, this sensitivity to fluctuations in turn impairs its specificity. Therefore, the presence of a subcritical component counterbalances this impairment.

Finally, we consider what may cause the difference in dynamics between the left and right dorsal habenula. Spontaneous activity is influenced by input. The dorsal left habenula, but not the right, receives an input from the thalamus.[41] Intrinsic activity in the thalamus may thus influence the left dorsal habenula. Spontaneous activity is also generated by intrinsic properties of the habenula neurons. In mammals, cholinergic neurons of the medial habenula exhibit regular tonic firing,[42,43] rather than sporadic activity. Cholinergic neurons are broadly expressed in the dorsal right habenula of zebrafish larvae.[44] If they exhibit similar properties as the rodent neurons, this would affect the overall dynamics of the right dorsal habenula. Thus, a combination of intrinsic and extrinsic factors may serve to give rise to the asymmetry in dynamics of the zebrafish dorsal habenula.

Methods

Ethical Statement.

Experiments were carried out using protocols approved by the IACUC of Biopolis, Singapore (# 171215).

Microscopy and Image Processing.

Calcium imaging was carried out on a Nikon A1R-MP two-photon system attached to a FN1 microscope with a 25x water dipping objective. Fish expressing GCaMP6s under the control of the s1011tGAL4 driver,[45] i.e. *Et(-1.5hsp70l:Gal4-VP16)s1011t, Tg(5xUAS:GCaMP6s)sq205*, were anesthetized in mivacurium, then embedded dorsal up in 2 percent agarose in a glass bottom dish (MatTek). The Ti-Sapphire laser was tuned to 930 nm, and images were collected using a galvano scanner.

The fluorescence time-series were motion corrected using the NoRMCorre algorithm contained in the CaImAn package.[46,47] Afterwards, neurons were manually identified as regions-of-interest (ROIs) via Fiji.[48,49] For each recording, 3 additional ROIs were extracted from regions that remain completely dark throughout the recording (i.e. with no apparent fluorescence).

The average of these fluorescence intensities provides a measure of the background intensity. We then computed $\Delta F/F = (F - F_0)/F_0$, where F and F_0 refer to average ROI and background intensity respectively, which is fed into the MLspike package, a Matlab-based spike inference package.[50] MLspike parameters are input according to known values for the fluorescence indicator gCaMP6s.[50]

Statistical Processing for Neural Avalanches.

In a population of neurons, spikes occurring in consecutive time steps form a cluster defined as an avalanche. We define an activity threshold λ_{thr}, where we only consider neural spikes that occur above the threshold. We expect the number of avalanches to remain relatively few at both small and large values of λ_{thr}: at small λ_{thr} spikes occur more often, which would form a small number of large avalanches; while for large λ_{thr}, a sparser set of spikes can yield but a small number of avalanches. We would expect, therefore, that a λ_{thr} value in between the two extremes would yield the largest number of avalanches. As the power law exponent has been shown to be robust with respect to changes in λ_{thr},[51] we optimize λ_{thr} as a way to increase the avalanche sample size.

From these thresholded spikes, we are then able to construct histograms of avalanche sizes and durations. To further increase the avalanche sample size, we combined histograms for recordings of the same sampling rate (number of recordings $-$ 2.0 Hz: 2, 3.6 Hz: 4, 7.0 Hz: 3, 13.0 Hz: 3). This is achieved by simply summing the counts for each histogram bin.

The effect of noise on the data is reduced by binning. We employ a logarithmic binning scheme most commonly used in the study of self-organized critical systems,[52] where the counts are averaged before being added into their corresponding bins as such:

$$P(b_j) = \frac{1}{b_j - b_{j-1}} \sum_i y_i, \tag{7}$$

where $b_j = R^j$ denotes the j-th bin (here we take $R = 1.7$), and y_i denotes the number of observations present in the interval $[b_{j-1}, b_j)$. When plotted, the bin counts are placed on the midpoint of the bin in logscale, i.e. $R^{j-1/2}$.

Power Law Fitting.

The power law exponents were computed by numerically solving a maximum likelihood equation:[53]

$$\sum_i P(x_i) \log x_i = \left(\sum_i x_i^{-\lambda} \right)^{-1} \sum_i x_i^{-\lambda} \log x_i, \quad (8)$$

where λ denotes the power law exponent, and x_i the i-th observation. The KS statistic D of each fit, which is a way to measure the distance between empirical data and its fit, was then computed via:[31]

$$D = \max_{x \geq x_{min}} |S(x) - P(x)|, \quad (9)$$

where $S(x)$ and $P(x)$ are the cumulative distribution function of the empirical data and fit distribution respectively, and x_{min} denotes the minimum x value above which lies the power law regime. The corresponding goodness of fit was then evaluated by comparing the KS statistics of the fit against synthetic power law data.[31] The likelihood ratio test was also conducted in the manner proposed by the same paper,[31] using discrete power law distribution $f(x) = x^{-\alpha}/\zeta(\alpha, x_{min})$ and discrete exponential distribution $f(x) = (1 - e^{-\lambda})e^{\lambda x_{min}} e^{-\lambda x}$ as candidate distributions. As binned exponential distribution is not well-resolved by the likelihood ratio test, this test is conducted on the unbinned data.

Mean Avalanche Size as a Function of Duration.

For $\langle S \rangle(T)$ plots, which defines a function and not a distribution, we fit a power law function using the scipy `theilslopes` function, which computes the Theil-Sen estimator for a given data. This method is preferred over the least-squares method owing to its robustness against outliers.

Shape collapse.

Shape collapse was achieved by following an established workflow.[29] In theory, we expect that the average number of spikes $s(t, T)$ for an avalanche of duration T at time t collapses to a universal parabolic shape when plotted as $s(t, T)T^{-\gamma}$ in the scale of normalized duration t/T for some exponent γ. We then optimized γ by minimizing the shape collapsed error, defined to be the mean variance divided by the range squared. To allow for such computations, $s(t, T)$ for each duration T was linearly interpolated to 1000 points. Here we consider only avalanches lasting at least 5 time steps and occurring at least 25 times.

All computations described above were done in Python. Algorithms where no specific function or package was mentioned were adapted as custom Python code.

References

1. Getting, P. A. Emerging principles governing the operation of neural networks. *Annual review of neuroscience* **12**, 185–204 (1989).
2. Marder, E. Neuromodulation of neuronal circuits: back to the future. *Neuron* **76**, 1–11 (2012).
3. Bargmann, C. I. & Marder, E. From the connectome to brain function. *Nature methods* **10**, 483 (2013).
4. Stephenson-Jones, M., Floros, O., Robertson, B. & Grillner, S. Evolutionary conservation of the habenular nuclei and their circuitry controlling the dopamine and 5-hydroxytryptophan (5-ht) systems. *Proceedings of the National Academy of Sciences* **109**, E164–E173 (2012).
5. Zhang, B.-b., Yao, Y.-y., Zhang, H.-f., Kawakami, K. & Du, J.-l. Left habenula mediates light-preference behavior in zebrafish via an asymmetrical visual pathway. *Neuron* **93**, 914–928 (2017).
6. Cheng, R.-K., Krishnan, S., Lin, Q., Kibat, C. & Jesuthasan, S. Characterization of a thalamic nucleus mediating habenula responses to changes in ambient illumination. *BMC biology* **15**, 104 (2017).
7. Matsumoto, M. & Hikosaka, O. Lateral habenula as a source of negative reward signals in dopamine neurons. *Nature* **447**, 1111 (2007).
8. Hong, S. & Hikosaka, O. The globus pallidus sends reward-related signals to the lateral habenula. *Neuron* **60**, 720–729 (2008).
9. Amo, R. *et al.* The habenulo-raphe serotonergic circuit encodes an aversive expectation value essential for adaptive active avoidance of danger. *Neuron* **84**, 1034–1048 (2014).
10. Baño-Otálora, B. & Piggins, H. D. Contributions of the lateral habenula to circadian timekeeping. *Pharmacology Biochemistry and Behavior* (2017).
11. Authement, M. E. *et al.* A role for corticotropin-releasing factor signaling in the lateral habenula and its modulation by early-life stress. *Sci. Signal.* **11**, eaan6480 (2018).
12. Wang, R. Y. & Aghajanian, G. K. Physiological evidence for habenula as major link between forebrain and midbrain raphe. *Science* **197**, 89–91 (1977).

13. Jhou, T. C., Fields, H. L., Baxter, M. G., Saper, C. B. & Holland, P. C. The rostromedial tegmental nucleus (rmtg), a gabaergic afferent to midbrain dopamine neurons, encodes aversive stimuli and inhibits motor responses. *Neuron* **61**, 786–800 (2009).

14. Thornton, E. W. & Bradbury, G. E. Effort and stress influence the effect of lesion of the habenula complex in one-way active avoidance learning. *Physiology & behavior* **45**, 929–935 (1989).

15. Lee, A. *et al.* The habenula prevents helpless behavior in larval zebrafish. *Current biology* **20**, 2211–2216 (2010).

16. Agetsuma, M. *et al.* The habenula is crucial for experience-dependent modification of fear responses in zebrafish. *Nature neuroscience* **13**, 1354 (2010).

17. Krishnan, S. *et al.* The right dorsal habenula limits attraction to an odor in zebrafish. *Current Biology* **24**, 1167–1175 (2014).

18. Lin, Q. *Using vertical migration of larval zebrafish to study non-image-forming light processing: Opsin, neural circuits and neuromodulators*. Ph.D. thesis, National University of Singapore (2015).

19. Jetti, S. K., Vendrell-Llopis, N. & Yaksi, E. Spontaneous activity governs olfactory representations in spatially organized habenular microcircuits. *Current biology* **24**, 434–439 (2014).

20. Fore, S., Palumbo, F., Pelgrims, R. & Yaksi, E. Information processing in the vertebrate habenula. In *Seminars in cell & developmental biology*, vol. 78, 130–139 (Elsevier, 2018).

21. Fosque, B. F. *et al.* Labeling of active neural circuits in vivo with designed calcium integrators. *Science* **347**, 755–760 (2015).

22. Beggs, J. M. & Plenz, D. Neuronal avalanches in neocortical circuits. *Journal of neuroscience* **23**, 11167–11177 (2003).

23. Kinouchi, O. & Copelli, M. Optimal dynamical range of excitable networks at criticality. *Nature physics* **2**, 348 (2006).

24. Shew, W. L., Yang, H., Petermann, T., Roy, R. & Plenz, D. Neuronal avalanches imply maximum dynamic range in cortical networks at criticality. *Journal of neuroscience* **29**, 15595–15600 (2009).

25. Shew, W. L. & Plenz, D. The functional benefits of criticality in the cortex. *The neuroscientist* **19**, 88–100 (2013).

26. Shew, W. L., Yang, H., Yu, S., Roy, R. & Plenz, D. Information capacity and transmission are maximized in balanced cortical networks with neuronal avalanches. *Journal of neuroscience* **31**, 55–63 (2011).

27. Sethna, J. P., Dahmen, K. A. & Myers, C. R. Crackling noise. *Nature* **410**, 242 (2001).

28. Friedman, N. *et al.* Universal critical dynamics in high resolution neuronal avalanche data. *Physical review letters* **108**, 208102 (2012).

29. Marshall, N. *et al.* Analysis of power laws, shape collapses, and neural complexity: new techniques and matlab support via the ncc toolbox. *Frontiers in physiology* **7**, 250 (2016).

30. Zapperi, S., Lauritsen, K. B. & Stanley, H. E. Self-organized branching processes: mean-field theory for avalanches. *Physical review letters* **75**, 4071 (1995).

31. Clauset, A., Shalizi, C. R. & Newman, M. E. Power-law distributions in empirical data. *SIAM review* **51**, 661–703 (2009).

32. Newman, M. E. Power laws, pareto distributions and zipf's law. *Contemporary physics* **46**, 323–351 (2005).

33. Stumpf, M. P. & Porter, M. A. Critical truths about power laws. *Science* **335**, 665–666 (2012).

34. Gleeson, J. P. & Durrett, R. Temporal profiles of avalanches on networks. *Nature Communications* **8**, 1227 (2017).

35. Haldeman, C. & Beggs, J. M. Critical branching captures activity in living neural networks and maximizes the number of metastable states. *Physical review letters* **94**, 058101 (2005).

36. Levina, A. & Priesemann, V. Subsampling scaling. *Nature communications* **8**, 15140 (2017).

37. Dreosti, E., Llopis, N. V., Carl, M., Yaksi, E. & Wilson, S. W. Left-right asymmetry is required for the habenulae to respond to both visual and olfactory stimuli. *Current Biology* **24**, 440–445 (2014).

38. Hendricks, M. & Jesuthasan, S. Asymmetric innervation of the habenula in zebrafish. *Journal of Comparative Neurology* **502**, 611–619 (2007).

39. Duboué, E. R., Hong, E., Eldred, K. C. & Halpern, M. E. Left habenular activity attenuates fear responses in larval zebrafish. *Current Biology* **27**, 2154–2162 (2017).

40. Gollo, L. L. Coexistence of critical sensitivity and subcritical specificity can yield optimal population coding. *Journal of The Royal Society Interface* **14**, 20170207 (2017).

41. Cheng, R.-K., Krishnan, S., Lin, Q., Kibat, C. & Jesuthasan, S. Characterization of a thalamic nucleus mediating habenula responses to changes in ambient illumination. *BMC biology* **15**, 104 (2017).

42. Kim, U. & Chang, S.-Y. Dendritic morphology, local circuitry, and intrinsic electrophysiology of neurons in the rat medial and lateral habenular nuclei of the epithalamus. *Journal of Comparative Neurology* **483**, 236–250 (2005).

43. Görlich, A. *et al.* Reexposure to nicotine during withdrawal increases the pacemaking activity of cholinergic habenular neurons. *Proceedings of the National Academy of Sciences* 201313103 (2013).

44. Hong, E. *et al.* Cholinergic left-right asymmetry in the habenulo-interpeduncular pathway. *Proceedings of the National Academy of Sciences* **110**, 21171–21176 (2013).

45. Scott, E. K. & Baier, H. The cellular architecture of the larval zebrafish tectum, as revealed by gal4 enhancer trap lines. *Frontiers in neural circuits* **3**, 13 (2009).

46. Giovannucci, A. *et al.* Caiman: An open source tool for scalable calcium imaging data analysis. *bioRxiv* 339564 (2018).

47. Pnevmatikakis, E. A. & Giovannucci, A. Normcorre: An online algorithm for piecewise rigid motion correction of calcium imaging data. *Journal of neuroscience methods* **291**, 83–94 (2017).

48. Schindelin, J. *et al.* Fiji: an open-source platform for biological-image analysis. *Nature methods* **9**, 676 (2012).

49. Schindelin, J., Rueden, C. T., Hiner, M. C. & Eliceiri, K. W. The imagej ecosystem: an open platform for biomedical image analysis. *Molecular reproduction and development* **82**, 518–529 (2015).

50. Deneux, T. *et al.* Accurate spike estimation from noisy calcium signals for ultrafast three-dimensional imaging of large neuronal populations in vivo. *Nature communications* **7**, 12190 (2016).

51. Bellay, T., Klaus, A., Seshadri, S. & Plenz, D. Irregular spiking of pyramidal neurons organizes as scale-invariant neuronal avalanches in the awake state. *Elife* **4**, e07224 (2015).

52. Pruessner, G. *Self-organised criticality: theory, models and characterisation*, chap. 7, 210–240 (Cambridge University Press, 2012).

53. Hanel, R., Corominas-Murtra, B., Liu, B. & Thurner, S. Fitting power-laws in empirical data with estimators that work for all exponents. *PloS one* **12**, e0170920 (2017).

Acknowledgements

This research was supported by the Singapore Ministry of Education under its Academic Research Fund Tier 1 (Project No. 2016-T1-001-152) to SJ and LYC, and an NGS Fellowship to MR.

Author contributions

S carried out data analysis and modeling with guidance from CLY. MR and SJ performed two-photon imaging. The project was designed by SJ and CLY.

Additional information

Supplementary Information accompanies this paper at URL.

Competing interests: The authors declare no competing financial interests.